Electronic continua in time-resolved photoelectron spectroscopy. II. Corresponding ionization correlations

M. Schmitt, S. Lochbrunner,[a] J. P. Shaffer, J. J. Larsen,[b] M. Z. Zgierski, and Albert Stolow[c]
Steacie Institute for Molecular Sciences, National Research Council of Canada, Ottawa, Ontario K1A 0R6, Canada

(Received 14 June 2000; accepted 20 October 2000)

We investigate further the role of ion electronic continua in time-resolved photoelectron spectroscopic measurements of ultrafast nonadiabatic coupling. In the preceding paper [Blanchet, Zgierski, and Stolow, J. Chem. Phys. **114**, 1194 (2000)], the limiting case of complementary ionization correlations permitted a disentangling of electronic from vibrational dynamics. Here we examine the other limiting case in which the nonadiabatically coupled sates (e.g., S_2 and S_1) correlations correspond to the same ionic continua, presumably an unfavorable case. We use ultrafast internal conversion in the polyaromatic hydrocarbons phenanthrene and naphthalene as examples. In this situation, the geometry changes (displacements) upon nonadiabatic crossing and upon ionization will strongly affect the ability to disentangle electronic from vibrational dynamics. Particularly, phenanthrene and naphthalene are both very rigid molecules and have small displacements upon internal conversion and ionization, still allowing for direct monitoring of the S_2 state internal conversion rate. © *2001 American Institute of Physics.* [DOI: 10.1063/1.1331637]

I. INTRODUCTION

The nonadiabatic coupling of electronic and vibrational degrees of freedom is central to much of the photochemistry of polyatomic molecules.[1] The investigation of nonradiative decay processes such as internal conversion and intersystem crossing has been the subject of intense research over many years.[2–9] The inherently rapid mixing of electronic with vibrational degrees of freedom leads to strongly varying transition moments and complex, often large amplitude nuclear dynamics. Here we consider the use of time domain techniques in which coherent superpositions of molecular eigenstates prepare the essentially zeroth-order states of interest.[10]

The choice of the final state in femtosecond pump–probe experiments is important as it affects the information content and determines the experimental method (e.g., detection of photons versus particles). The particular choice of the molecular ionization continuum as the final state is advantageous[11–16] because the ground state of the ion is often well known, ionization is a universal detection method (no ''dark'' states), and differential techniques (such as photoelectron spectroscopy) may be employed, increasing the information content.

Femtosecond time-resolved photoelectron spectroscopy (for a recent review, see Ref. 17) has been applied to wave packet dynamics in simple systems,[12,13,18–20] nonadiabatic intramolecular[11,21–28] and photodissociation[23,29] dynamics, spin–orbit coupling dynamics,[30,31] intracluster reaction dynamics,[32] excited state proton transfer dynamics,[33] and model molecular switches.[34] The outgoing photoelectron may be differentially analyzed as a function of time not only with respect to kinetic energy but also with respect to angular distributions[35–40] and spin polarization.[41] Additionally, time-resolved photoelectron–photoion coincidence[28] and photoelectron–photoion coincidence-imaging spectroscopies[29] have been demonstrated.

In this paper, we consider further the role of the ion core electronic continua in time-resolved photoelectron spectroscopy. In the preceding paper [Blanchet, Zgierski, and Stolow[42] (BZS)], we investigated the limiting case of complementary ionization correlations in which the coupled electronic excited states correlate with different ion core electronic states. The role of correlations upon photoionization was considered in a study of electronic population dynamics during intersystem crossing.[30] We demonstrated that these correlations could be used to disentangle electronic from vibrational dynamics during nonadiabatic processes.[23,24,26,42] This is discussed in detail in BZS.

Here, we study the other limiting case, that of corresponding ionization correlations in which the coupled electronic states (e.g., S_2 and S_1) correlate upon photoionization with the same electronic state of the ion (e.g., the ground state D_0). We expect such correlations to be unfavorable for disentangling electronic from vibrational dynamics. Nevertheless, nonadiabatic processes convert electronic to vibrational energy and the change in the latter could still be apparent in the photoelectron spectra. However, our ability to monitor the vibrational dynamics in each of the coupled electronic states depends strongly and specifically on the geometry changes (displacements) between the nonadiabatically coupled states and that of the ion state. In order to provide examples with corresponding ionization correlations and to

[a]Present address: Institut für Medizinische Optik, Ludwig-Maximilians-Universität München, D-80538 München, Germany.
[b]Present address: Institutes of Physics and Astronomy, University of Århus, DK-8000 Århus C, Denmark.
[c]Author to whom correspondence should be addressed. Electronic mail: albert.stolow@nrc.ca

TABLE I. Molecular orbital configuration in phenanthrene.

Electronic state	Molecular orbital occupancy						Weight	Correlated ion state
	a_2	a_2	b_1	a_2	b_1	b_1		
Neutral								
$S_0\ ^1A_1$	2	2	2	0	0	0	100%	$D_0\ ^2B_1$
$S_1\ ^1A_1$	2	2	1	0	1	0	50%	$D_0\ ^2B_1$
	2	1	2	1	0	0	50%	$D_1\ ^2A_2$
$S_2\ ^1B_2$	2	2	1	1	0	0	75%	$D_0\ ^2B_1$
	2	1	2	0	1	0	25%	$D_1\ ^2A_2$
Cation								
$D_0\ ^2B_1$	2	2	1	0	0	0	100%	
$D_1\ ^2A_2$	2	1	2	0	0	0	100%	
$D_2\ ^2A_2$	1	2	2	0	0	0	100%	

illustrate the effects discussed previously, we have chosen to study ultrafast internal conversion in the polyaromatic hydrocarbon phenanthrene and compare this behavior with that of naphthalene.

In Table I the molecular orbital configuration and approximate weights are shown for the electronic states of phenananthrene which are important in the internal conversion process. These were obtained with the QCFF/CISD method.[43,44] The ground S_0 state is a single configuration while the S_1 and the S_2 states consist of two configuration with a 1:1 and 3:1 weight, respectively. Within the Koopmans picture, ionic states are populated by single-photon, single active electron ionization. The result of this approximation is shown in the last column of Table I, which gives the ionic states formed upon adiabatic removal of the outermost electron. It can be seen that in the case of phenanthrene, both the S_2 and the S_1 states correlate with the ground state of the cation as well as the first excited state of the cation. This is the limiting case of corresponding ionization correlations and is to be contrasted with the limiting case of complementary ionization correlations discussed in BZS. In this paper, we show that even in this unfavorable case, time-resolved photoelectron spectroscopy can be applied in order to directly monitor the S_2 to S_1 internal conversion process. The ability to do this depends upon geometry changes in the molecule of interest. The results obtained on phenanthrene will be compared with those of naphthalene, which shows the same Koopmans-type correlations as phenanthrene. The main difference in the electronic level structure between phenanthrene and naphthalene is the energy gap between the S_2 and the S_1 states. Phenanthrene, which has a fairly large energy gap, belongs to the statistical limit case whereas naphthalene, with a smaller energy gap, corresponds to the intermediate coupling case.[45–53] These differences are further discussed in the following.

The optical transition prepares a zeroth-order electronic state (e.g., S_2) that is selected by its respective oscillator strength from the ground or initial state.[2,5,6,54,55] Isoenergetic with the optically bright state is a dense manifold of vibronic levels which belong to some lower zeroth-order electronic state (e.g., S_1). It is assumed that optical transitions between the initial state and this vibronic manifold are forbidden. The nonadiabatic coupling of the bright electronic state with the dense manifold of zeroth-order S_1 vibronic levels leads to the nonradiative ''decay'' (dephasing) of the zeroth-order S_2 wave packet. If the energy gap between these two excited states is big, the density of S_1 vibronic levels is extremely large and the dark state forms an apparently smooth quasicontinuum. Such a situation is known as the statistical limit for the radiationless transition problem. The very small and unequal level spacings mean that the revival time of the initially prepared state is very long compared to other time scales and therefore the dephasing of the initially prepared zeroth-order state appears irreversible. By contrast, if the electronic energy gap is comparable to the vibronic energy spacing, the S_1 vibronic states often form a highly structured manifold which is known as the intermediate case. The statistical limit is phenomenologically characterized by Lorentzian-type absorption bands where the apparent homogeneous width Γ is related to the 'lifetime' of the bright state, $\tau=\hbar/\Gamma$. In the intermediate case, a complex structured absorption spectrum with a broad energy spread obtains and, due to the larger level spacings in this case, very fast (usually nonexponential) nonradiative decay of the initial S_1/S_2 mixture is observed.

In the following, we describe our experimental method and then present our TRPES studies of internal conversion for the case of corresponding ionization correlations in phenanthrene and naphthalene.

II. EXPERIMENT

The experimental apparatus, described in detail elsewhere,[56,57] relies on a amplified femtosecond laser system to generate independently tunable UV pump and probe pulses and a high intensity molecular beam version of a magnetic bottle photoelectron spectrometer.

Briefly, for these experiments, the laser system consisted of a Ti:sapphire oscillator (830 nm, 75 fs) pumped by a diode-pumped based YLF laser. These pulses seeded a 1 kHz regenerative amplifier, resulting in 1.1 mJ pulses of 80 fs duration. The amplified 830 nm output was split into two, with a 30:70 ratio. Fourth-harmonic generation of the weaker beam by two successive BBO crystals provided UV probe pulses at 207.5 nm. The stronger beam was used to pump a four-pass optical parametric amplifier, the output of which

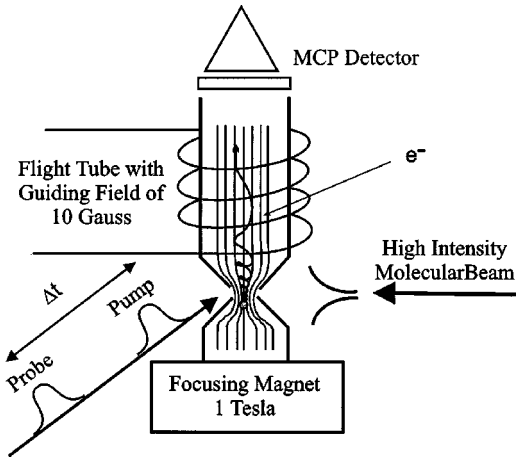

FIG. 1. Schematic sketch of the magnetic bottle photoelectron spectrometer. A skimmed molecular beam enters the interaction region of the magnetic bottle. The strongly divergent 1 T magnetic field parallelizes electron trajectories in the upper-half plane. These are guided in a 10 G field toward a detector. In a typical experiment, photoelectron kinetic energy spectra are recorded as a function of time delay.

was mixed with residual pump light at 830 nm to produce tunable pulses in the visible region (500–600 nm). These were frequency doubled in a thin BBO crystal to produce the UV pump pulses. Both the pump and probe pulses were recompressed in a double-prism configuration. The pump pulse was sent through a computer controlled optical delay line, recombined collinearly with the probe pulse, and focused by a 500 mm focal length mirror into the ionization region of the magnetic bottle time-of-flight spectrometer. Typical energies at the entrance to the chamber are 550 nJ in the probe beam and up to 2.0 μJ in the pump beam. Intensities were kept below 1×10^{11} W/cm^2 and therefore ponderomotive broadening of the spectra was neglible.[58] The absolute pump–probe $\Delta t=0$ and laser cross-correlation width were determined by difference frequency mixing of the pump and probe pulses in a BBO crystal directly in front of the chamber and by *in situ* nonresonant ionization of a simple gas (e.g., Xe). The cross-correlation signal between pump and probe laser was determined to be ~170 fs full width at half maximum (FWHM). In these experiments, both phenanthrene and naphthalene were each prepared by a fs pump pulse to be at the vibrationless electronic origin of their respective S_2 states.

The large, main high throughput source chamber (pumping speed 10 000 l/s, base pressure 2×10^{-7} Torr) is separated by two skimmers (0.3 and 1.0 mm diameter) from the ultrahigh vacuum magnetic bottle chamber (base pressure 2×10^{-10} Torr). A schematic sketch of the spectrometer is shown in Fig. 1. It is basically composed of a 1 T electromagnet, a solenoidal magnetic guiding field (10 G) along the drift tube, and a detector. The electrons initially emitted into the upper half-plane are parallelized by the highly divergent strong magnetic field at the interaction point, leading to a 2π solid angle collection.[59] The simple time-of-flight (TOF) measurement permitted each laser shot to be rapidly transferred to a computer for dynamic background subtraction, real-time data normalization, and active laser pulse energy filtering. The photoelectron energy calibration was obtained via two-photon ionization of nitric oxide. Due to the cylindrical symmetry about the laser propagation direction, these measurements are angle integrated.

Phenanthrene (or naphthalene) molecules were seeded in He (200 Torr) and introduced through a 0.5 mm continuous molecular beam nozzle. The phenanthrene sample cell was heated to 80 °C, the gas line and the nozzle to 120 and 130 °C, respectively, to prevent plugging. The naphthalene sample reservoir was kept at a temperature of 60 °C, while the gas line and nozzle temperatures were 70 and 80 °C, respectively. The naphthalene and phenanthrene were purchased from Aldrich and used without further purification.

III. RESULTS AND DISCUSSION

Considerable spectroscopic information is available about the energies and symmetries of the phenanthrene molecule and its cation, as summarized in Fig. 2(a) (see also Table I).[60] We excited jet-cooled phenanthrene from the $S_0(^1A_1)$ ground state to the origin of the $S_2(^1B_2)$ state with a 282 nm (4.39 eV) fs pump pulse. The excited molecules are then ionized after a time delay Δt using a 207.5 nm (5.98 eV) probe photon. The $S_2(^1B_2)$ state is known to rapidly internally convert to the lower lying $S_1(^1A_1)$ state at 3.64 eV, transforming electronic into vibrational energy (dashed line). The Koopmans-type correlations expected for single photon, single active electron ionization, as given in Table I, are shown by the downwards arrows. It can be seen that both the $S_2(^1B_2)$ and $S_1(^1A_1)$ states can correlate with the $D_0(^2B_1)$ ion ground state, producing the ϵ_1 and ϵ_4 photoelectron bands. They can also each correlate with the $D_1(^2A_2)$ ion excited state, producing the electron bands ϵ_2 and ϵ_5.

In Fig. 2(b) we show time-resolved photoelectron spectra for phenanthrene as a function of time delay between pump and probe pulses. The pump and the probe laser polarizations were parallel to the electron TOF axis. The photoelectron spectra reveal a rapidly decaying but energetically narrow peak at $\epsilon_1\approx2.5$ eV [see Fig. 2(b)]. This peak is due to photoionization of the vibrationless $S_2(^1B_2)$ state into the ionic ground state $D_0(^2B_1)$, as expected based on Table I. In order to monitor the zeroth-order electronic population decay in the S_2 state, i.e., to obtain its lifetime, this time-dependent peak in the photoelectron spectra was integrated and the integral plotted as a function of pump–probe delay time, as shown in Fig. 3. The solid line shown in Fig. 3 is a convolution of the pump–probe cross correlation of 170 fs (CC, dashed line) and a monoexponential decay. The fit results in a decay time constant of 522 ± 16 fs. The population flow out of the S_2 state is due to the population of high vibrational levels of the $S_1(^1A_1)$ state which are nonadiabatically coupled to the S_2 state (internal conversion).

The broad band, centered at about 1.5 eV, in these photoelectron spectra is partially due to ionization of vibrationally hot molecules in the S_1 state formed by the S_2–S_1 internal conversion. Normally one would expect this 1.5 eV band to grow as a function of time due to population flow into the S_1 state, as was demonstrated for the case of decateraene internal conversion[24,42] in BZS. This simple picture is

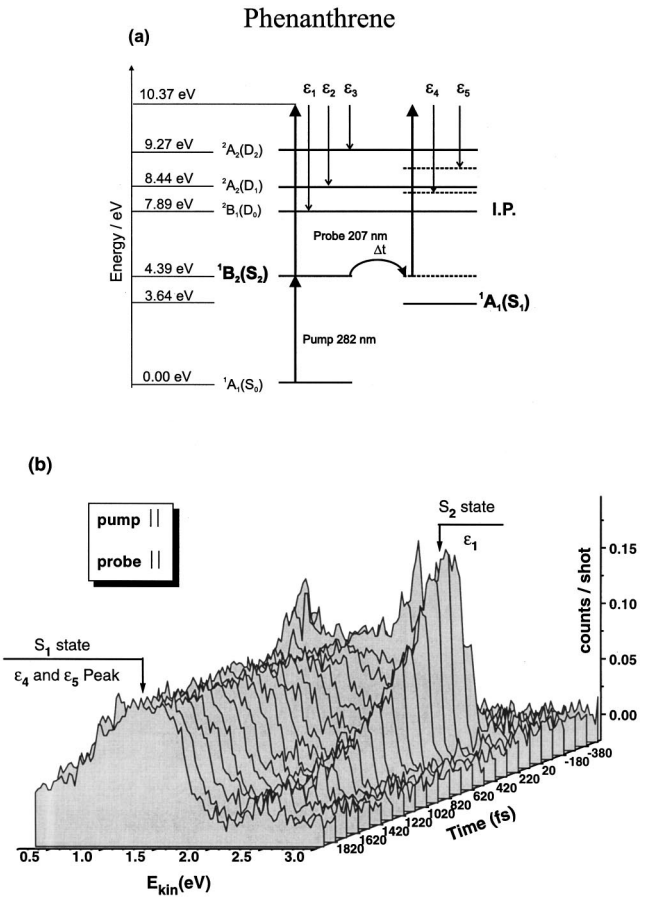

FIG. 2. Time-resolved vibrational and electronic dynamics during internal conversion for phenanthrene. (a) Energy level scheme for phenanthrene. Symmetry labels for the neutral and ionic states relevant to the time-resolved photoelectron spectra are given. As suggested in Table I, the S_2 state correlates electronically with the D_0 and D_1 producing the photoelectron bands ϵ_1 and ϵ_2. The S_1 state formed by internal conversion also correlates electronically with the D_0 and D_1, here producing the photoelectron bands ϵ_4 and ϵ_5. The dashed lines represent the vibrational energy in these states after internal conversion. (b) Time-resolved photoelectron spectra of phenanthrene for parallel pump and probe laser polarizations ($\lambda_{pump}=282$ nm, $\lambda_{probe}=207$ nm). The disappearance of the peak at $\epsilon_1=2.5$ eV represents a direct measure of the S_2-S_1 internal conversion time. The bands ϵ_4 and ϵ_5 are due to photoionization of S_1 into D_0 and D_1, respectively. For a discussion, see the text.

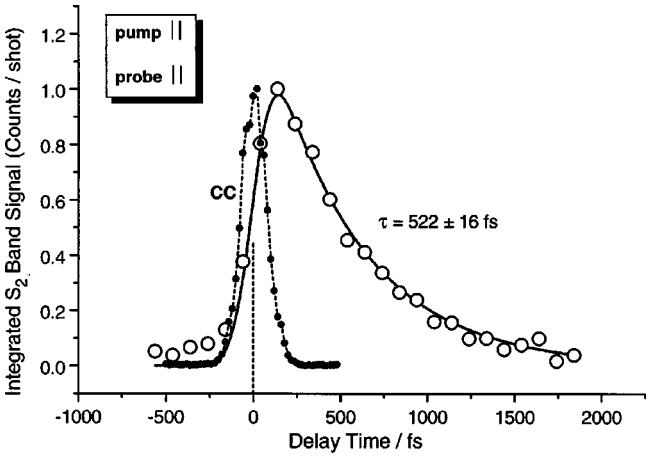

FIG. 3. Energy integration of the peak at $\epsilon_1=2.5$ eV shown in Fig. 2(b), plotted as a function of time. The solid line is a fit to a convolution of a monoexponential decay of time constant 522 ± 16 fs with a Gaussian cross-correlation function (CC, dashed line) of width 170 fs FWHM. This determines the S_2 lifetime to be 522 ± 16 fs.

not observed in our measurement because our probe laser has sufficient energy (5.98 eV) to project the intermediate state nonadiabatic wave packet produced by the pump laser onto several cation electronic states. Figure 2(a) shows that up to four photoionization bands ($\epsilon_2-\epsilon_5$) can in principle contribute to this 1.5 eV feature, although ionization out of the S_2 state into the second excited ionic state $D_1(\epsilon_3)$ should be less favorable because of the Koopmans propensity rules (see Table I). The broad component of the photoelectron spectra we observe around 1.5 eV is therefore, at short times, a superposition of both decaying (ϵ_2,ϵ_3) and growing (ϵ_4,ϵ_5) photoelectron bands. Generally one can expect that the photoelectron bands arising from ionization out of the S_1 state should be broader than those arising from the electronic origin of the S_2 state because of the ongoing intramolecular vibrational energy redistribution (IVR) in the vibrationally hot molecule on the S_1 potential energy surface. At times t >1500 fs or so (i.e., after internal conversion), the 1.5 eV band is comprised almost exclusively of signals due to S_1 ionization (ϵ_4 and ϵ_5). As can be seen, the S_1 state itself is long lived on the time scale of our experiment.[61]

As discussed in Sec. I, phenanthrene presents an example of the (unfavorable) limiting case of corresponding ionization correlations because both the S_2 and S_1 states can correlate electronically to the same ion electronic states (e.g., D_0). Despite this fact, we still see a dramatic shift in the photoelectron spectrum as a function of time, allowing us to directly monitor the electronic population flow. This is due to the fact that phenanthrene is a very rigid molecule and the S_2, S_1, and D_0 states all have roughly similar geometries. The photoionization probabilities are therefore expected to be dominated by small Δv transitions. This is illustrated by the calculated (QCFF/PI) Franck–Condon structures for the $S_{1,2}\rightarrow D_0$ and $S_{1,2}\rightarrow D_1$ transitions, shown in Figs. 4(a) and 4(b), respectively. The results are convoluted with a 75 meV instrumental width in order to match the experimental energy resolution, as in BZS. We can see that similar, short Franck–Condon progressions occur in $S_2\rightarrow D_0$ [Fig. 4(a), solid line], $S_1\rightarrow D_0$ [Fig. 4(b) dashed line], and $S_2\rightarrow D_1$ [Fig. 4(b), solid line] transitions. Only the $S_1\rightarrow D_1$ [Fig. 4(b), dashed line] transition is expected to show a somewhat longer progression, although even in this case, the 0–0 transition plays an important role in the spectrum. Hence, the 0.75 eV vibrational energy in the S_1 state would be roughly conserved upon ionization into the D_0 ionic state. That is to say, we would expect the edge of the ϵ_4 band to be shifted to lower energies by about 0.75 eV as compared with the ϵ_1 band. Indeed this is what is observed in Fig. 2(b). Therefore, for the particular case of phenanthrene, small geometry changes favor conservation of vibrational energy upon ionization and thereby permit the direct observation of the excited state electronic population dynamics via a photoelectron kinetic energy analysis. More generally, larger geometry changes upon internal conversion and ionization would mean that bands such as ϵ_1 and ϵ_4 would overlap, as was observed for

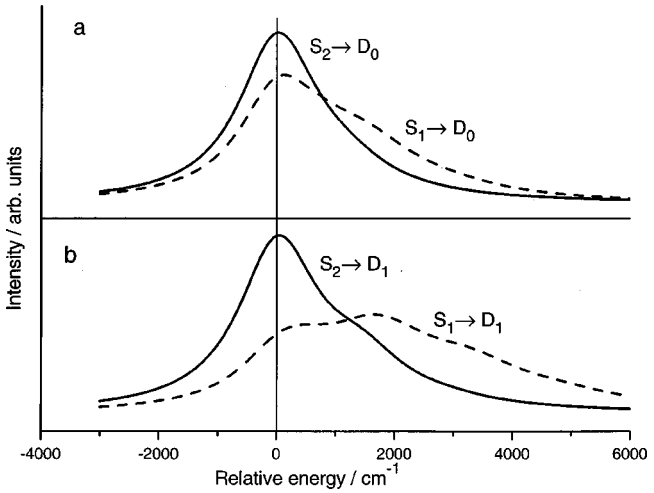

FIG. 4. Calculated QCFF/PI Franck-Condon structures for the $S_{1,2} \rightarrow D_0$ (a) and the $S_{1,2} \rightarrow D_1$ transition (b) in phenanthrene. The $S_2 \rightarrow D_0$ [(a), solid line] $S_1 \rightarrow D_0$ [(a), dashed line], and $S_2 \rightarrow D_1$ [(b), solid line] transitions show similar structure. Only the $S_1 \rightarrow D_1$ [(b), dashed line] transition shows a somewhat longer progression, although still showing a strong 0–0 transition (vertical solid line). The calculations have been convoluted with a 75 meV instrument function in order to match the experimental kinetic energy resolution.

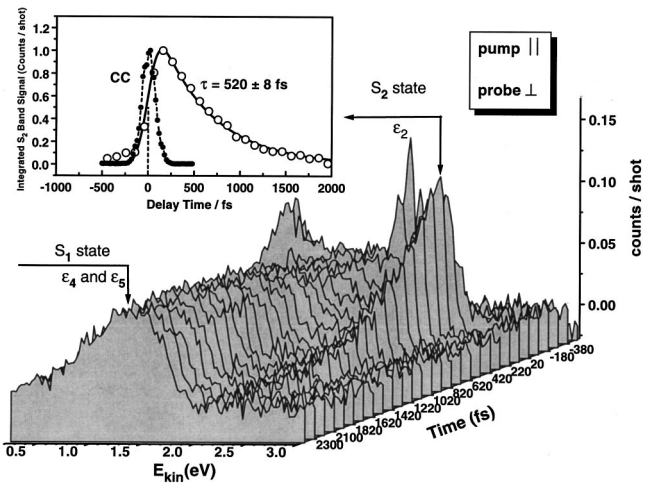

FIG. 5. Time-resolved photoelectron spectra of phenanthrene for perpendicular pump and probe laser polarizations ($\lambda_{pump} = 282$ nm, $\lambda_{probe} = 207$ nm). The disappearance of the peak at $\epsilon_1 = 2.5$ eV again represents a direct measure of the $S_2 - S_1$ internal conversion time and confirms the accuracy of the results shown in Fig. 2. The bands ϵ_4 and ϵ_5 are due to photoionization of S_1 into D_0 and D_1, respectively. (Inset) Energy integration of the peak at $\epsilon_1 = 2.5$ eV plotted as a function of time. The solid line is a fit to a convolution of a monoexponential decay of time constant 520 ± 8 fs with a Gaussian cross-correlation function (CC, dashed line) of width 170 fs FWHM. This determines the S_2 lifetime to be 520 ± 8 fs, confirming the accuracy of the results shown in Fig. 3.

the case of $S_1 - S_0$ internal conversion in hexatriene.[21] In such cases, a clear disentangling of electronic from vibrational dynamics is more challenging and requires a consideration of even more differential measurements, such as energy resolved photoelectron angular distributions.

Photoelectron spectra measured at perpendicular pump–probe polarizations can show different ionization cross sections than those measured with parallel pump–probe polarizations due to an aligned intermediate state. Figure 5 shows the photoelectron spectra obtained with perpendicular polarization between pump and probe laser. These photoelectron spectra are essentially identical to those obtained with parallel polarization [see Fig. 2(b)]. These observations indicate that the experimental measurements are insensitive to any intermediate state alignment and rotational dephasing effects. Rotational dephasing would otherwise be unexpected on the time scale of these measurements. In Fig. 5 (inset), we show the integrated $\epsilon_1 \approx 2.5$ eV peak (due to S_2 ionization into the D_0 continuum) as a function of time. The fit yields a decay time constant of 520 ± 8 fs. This agrees with the results from Fig. 3 within our experimental error bars and confirms the accuracy and reproducibility of these measurements.

The energy gap between the electronic origins of the S_2 and S_1 states is 0.75 eV. This value is sufficiently large to ensure that electronic ''relaxation'' from the S_2 state occurs in the statistical limit. The absorption and the fluorescence excitation spectra for the $S_0 \rightarrow S_2$ transition measured in a supersonic free jet revealed a Lorentzian-type spectral line shape.[52,53] In the statistical limit, the line shape is expected to appear Lorentzian with a homogeneous width related directly to the electronic dephasing time scale. From the observed linewidth the homogeneous width was estimated by deconvoluting the rotational broadening contribution. The latter was obtained from the inhomogeneously broadened $S_0 \rightarrow S_1$ origin by assuming that the rotational broadening is the same for both transitions. This estimated homogeneous width for phenanthrene was found to be 11.1 cm^{-1} and leads to an inferred internal conversion rate for the vibrationless level of the S_2 state in isolated phenanthrene molecules of $\sim$500 fs. This estimate based on linewidth measurement and rotational deconvolution can now be confirmed by the more accurate values we measured directly (Figs. 3 and 5). As discussed previously, the time-resolved photoelectron spectra [Figs. 2(b) and 5] directly reveal the $S_2 - S_1$ internal conversion time scale via the decay of the peak at $\epsilon_1 \approx 2.5$ eV. We note that linewidth measurements can give a good estimate of the electronic dephasing time scale but do not provide much information about the underlying nuclear dynamics. Although not apparent in phenanthrene due to the high density of states, time-resolved photoelectron spectroscopy can reveal the underlying vibrational dynamics which promotes and tunes the nonadiabatic crossing as well as the IVR which occurs on the ''dark'' potential energy surface,[24] as discussed in BZS.

While phenathrene shows narrow Lorentzian-type absorption or fluorescence excitation bands, naphthalene by contrast has a complicated, irregularly structured absorption spectrum above the S_2 threshold.[45,46,49] The structure cannot be assigned to a conventional vibrational progression and has been interpreted in terms of strong mixing of the zeroth-order vibronic states in the S_2 manifold with a sparse set of zeroth-order vibronic S_1 states.[45,46,48–50,62] In such cases, the mixing of zeroth-order S_2 with zeroth-order S_1 states depends on accidental degeneracies. The character of these molecular eigenstates can therefore fluctuate between those that are essentially S_2, those that are essentially S_1, and states that are on average an equal combination of both. These are

typical characteristics of the intermediate level structure case which is found in molecules with small S_2-S_1 energy gaps such as naphthalene [$\Delta E(S_2-S_1)=0.48$ eV]. If the vibronic level density in the S_1 state is low in the region of the electronic resonance, the spectrum is not broadened as in the statistical limit case but rather appears as a highly complex set of sharp lines. In this case the complete vibronic mixing of the S_2 state with the lower lying S_1 state leads to the loss of the identity of the S_2 state in the Born–Oppenheimer sense. The estimated degree of the zeroth-order vibrationless S_2 character in the region near the S_2 origin is only 10%–20%.[46,49] Vibrationally resolved photoelectron spectra of jet-cooled naphthalene, obtained via ionization from various vibronic levels of the S_1 and S_2 states, was previously reported.[51] Among other things addressed was the question of which electronic state the photoelectrons were ejected from in the case of the excitation to the S_2 origin. It was observed that the electronic dephasing rate is much faster than the ionization rate from the optically prepared zero-order S_2 state and that many vibrationally excited S_1 states are produced. The estimated S_2-S_1 dephasing rate was faster than $10^{11}\,s^{-1}$.

Naphthalene has the same limiting case Koopmans-type correlations as phenanthrene. An interesting question is how the intermediate case S_2-S_1 coupling in naphthalene manifests itself in time-resolved photoelectron measurements. In order to investigate this, we prepared the S_2 electronic origin with a fs pump pulse at 278 nm [see Fig. 6(a)]. As in phenanthrene, both S_2 and S_1 can ionize into D_0 producing the photoelectron bands ϵ_1 and ϵ_3, both S_2 and S_1 can ionize into D_1 producing the photoelectron bands ϵ_2 and ϵ_4. These dynamics lead to the time-resolved photoelectron spectra shown in Fig. 6(b). The spectra show a peak at $\epsilon_1=2.3$ eV, which is due to ionization of the $S_2(^1B_{2u})$ state into the $D_0(^2A_u)$ ground electronic state of the ion. Figure 7 shows the integrated 2.3 eV photoelectron peak (circles) from Fig. 6(b) as well as the laser cross-correlation signal (CC, dashed lines) measured by difference frequency mixing in a BBO crystal. It can be seen that this S_2 signal does not differ appreciably from the cross-correlation signal (for positive times). This observation means the S_2-S_1 internal conversion time must be considerably faster than 100 fs, as expected. These spectra also show an energetic band at $\epsilon_3=1.8$ eV arising from photoionization of vibrationally hot S_1 molecules into the $D_0(^2A_u)$ ionic ground state of the ion. The signal between 1.2 and 1.7 eV corresponds to ionization of the S_2 state into the $D_1(^2B_{1u})$ excited state of the ion. For time delays outside the cross correlation we find a constant signal between 0.6 and 1.8 eV which is due to ionization of the S_1 state (ϵ_3 and ϵ_4). Photoelectrons arising from ionization out of the S_2 state into the D_1 excited state of the ion having an energy of $\epsilon_2\approx 1.60$ eV do not contribute to this broad band because, as we see from the peak ϵ_1 which follows the cross-correlation signal, the S_2-S_1 internal conversion occurs within the cross-correlation time. This shows for nonoverlapping lasers that, only the S_1 state is populated. For negative delay times (i.e., pumping at 207.5 nm), decay dynamics of an unassigned higher lying state can be seen in Fig. 7.

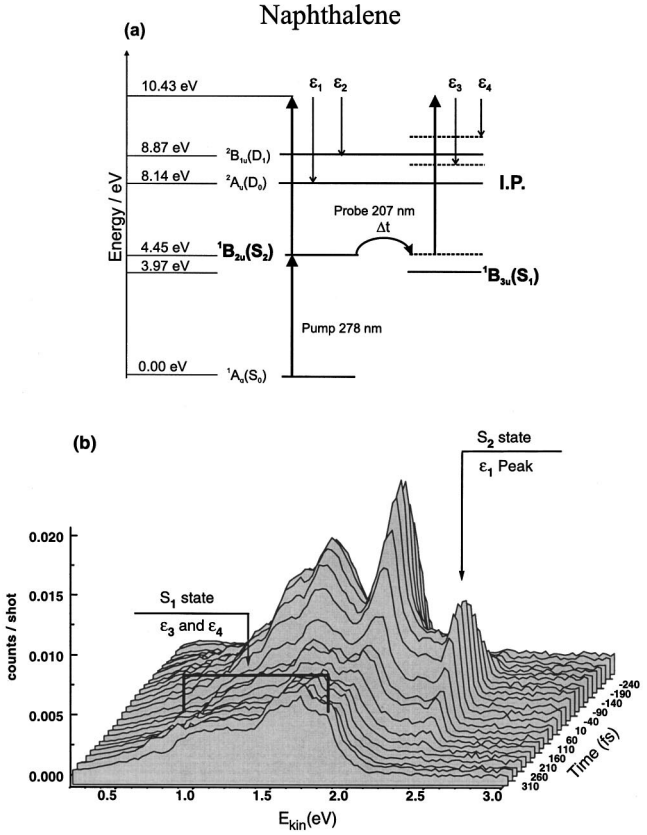

FIG. 6. Time-resolved vibrational and electronic dynamics during internal conversion for naphthalene. (a) Energy level scheme for naphthalene. Symmetry labels for the neutral and ionic states relevant to the time-resolved photoelectron spectra are given. As suggested in Table I for phenanthrene, the S_2 state correlates electronically with the D_0 and D_1 producing the photoelectron bands ϵ_1 and ϵ_2. The S_1 state formed by internal conversion correlates electronically with D_0 and D_1 producing the photoelectron bands ϵ_3 and ϵ_4. The dashed lines represent the vibrational energy in these states after internal conversion. (b) Time-resolved photoelectron spectra of naphthalene for parallel pump and probe laser polarizations ($\lambda_{pump}=278$ nm; $\lambda_{probe}=207$ nm). The peak at $\epsilon_1=2.3$ eV is due to photoionization of S_2 into D_0. The bands ϵ_3 and ϵ_4 are due to photoionization of the S_1 state into D_0 and D_1, respectively. The internal conversion time scale in this intermediate coupling case is faster than our time resolution.

The S_2 origin of naphthalene, which is a typical example of an intermediate coupling case, shows a much faster S_2-S_1 internal conversion than phenanthrene. The rate of internal conversion depends not only on the gap between the two interacting states but also on the vibronic coupling of the two states by promoting modes of b_2 symmetry for phenanthrene and b_{1g} symmetry for naphthalene. We have calculated these parameters previously for naphthalene using the complete neglect of differential overlap/S method using QCFF/PI normal modes.[63] Calculations done for phenanthrene in the same way reveal that the largest coupling, for the 1375 cm^{-1}C–C b_2 stretching mode, is 30 cm^{-1}. This is a factor of 2 smaller than the value of the largest S_2-S_1 coupling in naphthalene.[63] Therefore, the slower internal conversion in phenanthrene as compared with naphthalene is due to both a larger electronic energy gap and a smaller vibronic coupling strength between the two electronic states.

The characterization of nonradiative processes like internal conversion is described as a dephasing of molecular

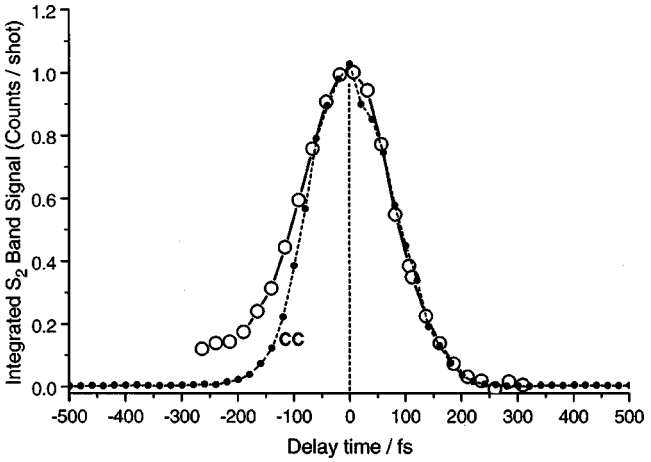

FIG. 7. Energy integration of the peak at $\epsilon_1 = 2.3$ eV shown in Fig. 6(b), plotted as a function of time. It can be seen that, for positive times, this signal follows the cross-correlation signal (CC, dashed line) indicating that the internal conversion time scale is much less than 100 fs. For negative time delays, the excited state dynamics of a higher lying state can be seen. For a discussion, see the text.

eigenstates.[5,54,55] The pump pulse coherently excites a wave packet, in the impulsive limit, with S_2 character. Immediately after the laser pulse, the phases of all eigenstates in the wave packet interfere constructively so as to augment S_2 character and interfere destructively with respect to S_1 character. This means that the photoelectron spectrum at the time of excitation shows a signal dominated by photoionization of the zeroth-order S_2 state. For longer delay times, dephasing of all the molecular eigenstates occurs, leading to a loss of S_2 character. If these states contain both S_2 and S_1 character, and the S_1 character dominates, then the dephasing process essentially converts a zero-order S_2 state into a zero-order S_1 state. The time required for this process is on the order of the reciprocal energy width over which the S_2 character is distributed. Our laser pulses were not short enough (i.e., did not have sufficient bandwidth $\Delta\omega$) to excite all eigenstates with S_2 contribution in naphthalene. This means that, in contrast to phenanthrene, the excitation does not in fact prepare the zeroth-order Born–Oppenheimer S_2 state and therefore we observe a dephasing time which is just $\sim\Delta\omega^{-1}$, the inverse laser bandwidth. (Due to the irregular level spacings in the problem, the revival of the zeroth-order S_2 state would take quite some time). Nevertheless, the molecular ionization continuum is still quite a useful template for projecting out zeroth-order electronic configurations, as can be seen from Fig. 6(b).

IV. CONCLUSION

In this paper, we investigated the role of different ion core electronic continua upon time-resolved photoelectron spectroscopy measurements. We have identified two limiting cases of photoionization correlations in such experiments. Specifically, in contrast to the preceding paper (BZS) where complementary ionization correlations permitted a disentangling of electronic from vibrational dynamics, here we considered the other limiting case of corresponding correlations where the nonadiabatically coupled excited states correlate with the same ion electronic states. In these situations, geometrical effects (displacements) become important for observing the electronic population flow. To this end, we have chosen the presumably unfavorable case of polyaromatic hydrocarbons where both the initial (S_2) and final (S_1) states correlate to the same electronic states of the ion (e.g., D_0). We investigated the S_2-S_1 internal conversion process in phenanthrene and, for comparison, in naphthalene. In phenanthrene, the electronic population flow out of the S_2 state, forming a vibrationally hot S_1 state, was directly observed with a time constant of 521 fs, confirming previous estimates based upon deconvoluted linewidth measurements. Phenanthrene is a rigid molecule with small displacements upon transitions. The direct observation of electron population flow was favored by the small geometry changes upon ionization (small Δv).

The S_2-S_1 internal conversion process in naphthalene, by contrast, occurred within the cross correlation of our laser pulses. The different dephasing times of phenanthrene and naphthalene can be understood in terms of the different S_2-S_1 energy gaps and coupling strengths in these two molecules. In phenanthrene the energy gap is 0.75 eV so the S_1 state forms an apparently smooth quasicontinuum, the statistical limit. In this case, the initially prepared S_2 state dephases irreversibly into this quasicontinuum with a rate constant given by the well-known Fermi golden rule rate expression. Naphthalene has a smaller S_2-S_1 energy gap (0.48 eV) and a vibronic coupling strength roughly double that of phenanthrene. In this case the S_1 state forms a highly structured ''quasicontinuum,'' known as the intermediate coupling case. Here the S_2 state is diluted among a manifold of spectroscopically distinct molecular eigenstates which are formed by the coupling. The mixing of S_2 with S_1 states leads to a very fast S_2-S_1 internal conversion process. In naphthalene, the bandwidth of our pump laser pulse is narrower than the spectral spread of molecular eigenstates containing S_2 character. In such cases, the observed electronic dephasing time is simply the inverse pump laser bandwidth.

In the most general case, neither the electronic correlations nor the geometry changes may be favorable. As an example, consider a case where the two coupled states correlate to the same ion states (e.g., D_0) and the geometry changes upon internal conversion and ionization are significant, leading to long, overlapping vibrational progressions. In this situation, photoelectron kinetic energy analysis alone will likely fail to disentangle electronic from vibrational dynamics. However, the other component of the ionization continuum, the free electron wave function, remains available for analysis. The free electron partial wave composition determines the photoelectron angular distribution (PAD). The symmetry of the PAD is determined by the electronic symmetry changes upon ionization and therefore it is expected that photoelectron angular distribution measurements reflect the evolution of excited state electronic symmetry during nonadiabatic processes. A general nonperturbative formalism for the calculation of time-resolved PADs has been developed.[36,39,40] In forthcoming paper,[64] we apply this formalism to several examples of excited state nonadiabatic dynamics and discuss the new opportunities which emerge

from these considerations. We expect time-resolved photoelectron spectroscopy to be of potential use whenever excited state nuclear dynamics leads to changes in the charge distribution of the molecule. As discussed in BZS, such processes include internal conversion, intersystem crossing, proton transfer, electron transfer, and molecular scale electronic switching. We anticipate seeing many new studies of such systems.

ACKNOWLEDGMENTS

The authors thank Professor C. A. de Lange, Professor W. J. Buma, and Professor V. Blanchet for helpful discussions on magnetic bottle photoelectron spectroscopy. M.S. and S.L. acknowledge the Deutsche Forschungsgemeinschaft for the receipt of a Postdoktoranden Stipendium. J.J.L. acknowledges the Danish government for financial support.

[1] J. Michl and J. Bonacic-Koutecky, *Electronic Aspects of Organic Photochemistry* (Wiley, New York, 1990).
[2] W. Siebrand, J. Chem. Phys. **47**, 2411 (1967).
[3] J. Jortner, S. A. Rice, and R. M. Hochstrasser, Adv. Photochem. **7**, 149 (1969).
[4] B. R. Henry and W. Siebrand, *Radiationless Transitions*, in Organic Molecular Photophysics Vol. 1, edited by J. B. Birks (Wiley, London, 1973).
[5] K. F. Freed, in *Radiationless Processes in Molecules and Condensed Phases*, edited by F. K. Fong (Springer, Berlin, 1976), pp. 23–168.
[6] W. Siebrand and M. Z. Zgierski, J. Chem. Phys. **75**, 1230 (1981).
[7] H. Koppel, W. Domcke, and L. S. Cederbaum, Adv. Chem. Phys. **57**, 59 (1984).
[8] M. Garavelli, P. Celani, N. Yamamoto, F. Bernardi, M. A. Robb, and M. Olivucci, J. Am. Chem. Soc. **118**, 11656 (1996).
[9] G. Stock and W. Domcke, Adv. Chem. Phys. **100**, 1 (1997).
[10] A. H. Zewail, *Femtochemistry: Ultrafast Dynamics of the Chemical Bond* (World Scientific, Singapore, 1994).
[11] M. Seel and W. Domcke, J. Chem. Phys. **95**, 7806 (1991).
[12] C. Meier and V. Engel, Chem. Phys. Lett. **212**, 691 (1993).
[13] I. Fischer, D. M. Villeneuve, M. J. J. Vrakking, and A. Stolow, J. Chem. Phys. **102**, 5566 (1995).
[14] I. Fischer, M. J. J. Vrakking, D. M. Villeneuve, and A. Stolow, in *Ultrafast Phenomena X*, edited by P. F. Barbara, J. G. Fujimoto, W. H. Know, and W. Zinth (Springer, Berlin, 1996), p. 187.
[15] I. Fischer, M. J. J. Vrakking, D. M. Villeneuve, and A. Stolow, Chem. Phys. **207**, 331 (1996).
[16] I. Fischer, D. M. Villeneuve, M. J. J. Vrakking, and A. Stolow, in *Femtochemistry: The Lausanne Conference*, edited by M. Chergui (World Scientific, Singapore, 1996), p. 43.
[17] C. C. Hayden and Albert Stolow, in *Photoionization and Photodetachment Advanced Series in Physical Chemistry*, Vol. 10, edited by C. Y. Ng (World Scientific, Singapore, 2000).
[18] T. Baumert, R. Thalweiser, and G. Gerber, Chem. Phys. Lett. **209**, 29 (1993).
[19] A. Assion, M. Geisler, J. Helbing, V. Seyfried, and T. Baumert, Phys. Rev. A **54**, R4605 (1996).
[20] B. J. Greenblatt, M. T. Zanni, and D. M. Neumark, Chem. Phys. Lett. **258**, 523 (1996).
[21] D. R. Cyr and C. C. Hayden, J. Chem. Phys. **104**, 771 (1996).
[22] W. Radloff, V. Stert, Th. Freudenberg, I. V. Hertel, C. Jouvet, C. Dedonder-Lardeux, and D. Solgadi, Chem. Phys. Lett. **281**, 20 (1997).
[23] V. Blanchet and A. Stolow, J. Chem. Phys. **108**, 4371 (1998).
[24] V. Blanchet, M. Z. Zgierski, T. Seideman, and A. Stolow, Nature (London) **401**, 52 (1999).
[25] C. P. Schick, S. D. Carpenter, and P. M. Weber, J. Phys. Chem. A **103**, 10470 (1999).
[26] V. Blanchet and A. Stolow, in *Ultrafast Phenomena XI*, edited by T. Elsaesser, J. G. Fujimoto, D. A. Wiersma, and W. Zinth (Springer, Berlin, 1998), p. 456.
[27] J. P. Shaffer, T. Schultz, M. Schmitt, and A. Stolow (unpublished).
[28] V. Stert, W. Radloff, C. P. Schulz, and I. V. Hertel, Eur. Phys. J. D **5**, 97 (1999).
[29] J. A. Davies, J. E. LeClaire, R. E. Continetti, and C. C. Hayden, J. Phys. Chem. **111**, 1 (1999).
[30] B. Kim, C. P. Schick, and P. M. Weber, J. Chem. Phys. **103**, 6903 (1995).
[31] T. Suzuki, L. Wang, and H. Kohguchi, J. Chem. Phys. **111**, 4859 (1999).
[32] B. J. Greenblatt, M. T. Zanni, and D. M. Neumark, Science **276**, 1675 (1997).
[33] S. Lochbrunner, J. P. Shaffer, M. Schmitt, T. Schultz, and A. Stolow (unpublished).
[34] T. Schultz, J. P. Shaffer, M. Schmitt, and A. Stolow (unpublished).
[35] K. L. Reid, S. P. Duxon, and M. Towrie, Chem. Phys. Lett. **228**, 351 (1994).
[36] T. Seideman, J. Chem. Phys. **107**, 7859 (1997).
[37] K. L. Reid, T. A. Field, M. Towrie, and P. Matousek, J. Chem. Phys. **111**, 1438 (1999).
[38] Y. Arasaki, K. Takatsuka, K. Wang, and V. McKoy, Chem. Phys. Lett. **302**, 363 (1999).
[39] S. C. Althorpe and T. Seideman, J. Chem. Phys. **110**, 147 (1999).
[40] T. Seideman, J. Chem. Phys. (submitted).
[41] M. Aeschlimann, M. Bauer, S. Pawlik, W. Weber, R. Burgermeister, D. Oberli, and H. C. Siegmann, Phys. Rev. Lett. **79**, 5158 (1997).
[42] V. Blanchet, M. Z. Zgierski, and A. Stolow, J. Chem. Phys. **114**, 1194 (2000).
[43] A. Warshel and M. Karplus, J. Am. Chem. Soc. **94**, 5612 (1972).
[44] F. Zerbretto, M. Z. Zgierski, F. Negri, and G. Orlandi, J. Chem. Phys. **89**, 3681 (1988).
[45] D. S. McClure, J. Chem. Phys. **22**, 1668 (1954).
[46] J. E. Wessel, Ph.D. thesis, University of Chicago, 1971.
[47] P. Wannier, P. M. Rentzepis, and J. Jortner, Chem. Phys. Lett. **10**, 193 (1971).
[48] C. A. Langhoff and G. W. Robinson, Chem. Phys. **6**, 34 (1974).
[49] J. E. Wessel and D. S. McClure, Mol. Cryst. Liq. Cryst. **58**, 121 (1980).
[50] S. M. Beck, D. E. Powers, J. B. Hopkins, and R. E. Smalley, J. Chem. Phys. **73**, 2019 (1980).
[51] A. Hiraya, Y. Achiba, N. Mikami, and K. Kimura, J. Chem. Phys. **82**, 1810 (1984).
[52] A. Amirav, M. Sonnenschein, and J. Jortner, J. Phys. Chem. **88**, 5593 (1984).
[53] N. Ohta and H. Baba, Mol. Phys. **59**, 921 (1986).
[54] M. Bixon and J. Jortner, J. Phys. Chem. **48**, 715 (1968).
[55] R. Engelmann and J. Jortner, Mol. Phys. **18**, 145 (1970).
[56] V. Blanchet, S. Lochbrunner, M. Schmitt, J. P. Shaffer, J. J. Larsen, M. Z. Zgierski, T. Seideman, and A. Stolow, Faraday Discuss. **115**, 33 (2000).
[57] S. Lochbrunner, J. J. Larsen, J. P. Shaffer, M. Schmitt, T. Schultz, J. G. Underwood, and A. Stolow, J. Electronic Spectrosc. Relat. Phenom. (in press).
[58] A. Zavriyev, I. Fischer, D. M. Villeneuve, and A. Stolow, Chem. Phys. Lett. **234**, 281 (1995).
[59] P. Kruit and F. H. Read, J. Phys. E **16**, 313 (1983).
[60] F. Salama, C. Joblin, and L. J. Allamandola, J. Chem. Phys. **101**, 10252 (1994).
[61] N. Thantu and P. M. Weber, Chem. Phys. Lett. **214**, 276 (1993).
[62] P. Wannier, P. M. Rentzepis, and J. Jortner, Chem. Phys. Lett. **10**, 193 (1971).
[63] F. Negri and M. Z. Zgierski, J. Chem. Phys. **104**, 3486 (1996).
[64] M. Schmitt, M. Z. Zgierski, A. Stolow, and T. Seideman, forthcoming paper.